ISSN 1070-4272, Russian Journal of Applied Chemistry, 2017, Vol. 90, No. 12, pp. 2055−2063. © Pleiades Publishing, Ltd., 2017.

VARIOUS TECHNOLOGICAL PROCESSES

Quinoline Hydrodenitrogenation over NiW/Al-MCM-41 Catalysts with Different Al Contents[1]

Fang Guo[a], Jun Li[a], Wanxi Li[a], Xiuling Chen[a], Hongxue Qi[a], Xiaoxiao Wang[b,*], and Yue Yu[c]

[a] *Jin Zhong University, College of Chemistry and Chemical Engineering, Yuci 030619, P. R. China*
[b] *Taiyuan University of Science and Technology, School of Chemical and Biological Engineering, Taiyuan 030024, P. R. China*
**e-mail: wang5203264@sina.com*
[c] *Lin Yi Academy of Technology Cooperation and Application, Linyi 276000, P. R. China*

Received November 12, 2017

Abstract—Al-MCM-41 materials were prepared with different Al contents and used as supports for NiW catalysts. The supports and catalysts were characterized by XRD, N_2 adsorption-desorption, XPS, Raman, H_2-TPR techniques. The XPS result showed that the Al added to MCM-41 promoted the dispersion of W and Ni species. The Raman result showed that the Al added to MCM-41 favored the formation of the suitable W species. The H_2-TPR result showed that the Al added to MCM-41 can reduce the reduction temperature of W species on the catalysts. The hydrodenitrogenation (HDN) results showed that the HDN activity followed the order of NiW/Al-2 > NiW/Al-1 > NiW/Al-4 > NiW. Moreover, this tendency was also valid for the ratio of propylcyclohexane/propylbenzene (PCH/PB). The high HDN activity and PCH/PB ratio of NiW/Al-2 are due to the well dispersion of the W and Ni species, the suitable W species and the low reduction temperature of W species.

DOI: 10.1134/S1070427217120242

INTRODUCTION

The conventional hydrodesulfurization (HDS) and hydrodenitrogenation (HDN) catalysts are alumina supported Mo or W sulfides promoted by Ni or Co. Generally, HDN is more difficult than HDS. In recent times, many efforts are aimed to enhance the catalytic activity of HDS and HDN catalysts. Among the approaches to achieve this goal, one approach is to choose proper support for the active components. It was found that the support can influence catalyst reducibility or sulfidability, structure and dispersion of the deposited metal oxides, as well as the morphology of the sulfided active phases [1–4].

The MCM-41 mesoporous molecular sieves materials, which have ordered pore structure and high surface area attracted much interest in the catalytic process. There are several reports available on HDS and HDN catalysts supported on MCM-41 materials [5–9]. Wang et al. [5] studied the support effect of MCM-41 for Co-Mo catalyst and found that MCM-41 is a good support for HDS of DBT. They developed high performance HDS catalysts by depositing Ni–Mo and Ni–W over MCM-41 [10, 11].

Generally, the incorporation of heteroatom and the amount of heteroatom play important role in the precursor structure of catalysts and in the activity. Some HDS and HDN studies have been made using MCM-41 modified with heteroatom, such as Al, Ti, Zr, and Nb [12–16]. In the previous paper [16], we have reported that Al, Zr, and Ti modified MCM-41, especially Al, can promote the activity in the HDN of quinoline. The effect of the amount of heteroatom on the HDS has also been analyzed in several studies [17, 18]. Souza et al. [17] reported the effect of Si/Al molar ratio of Al-MCM-41 support on the CoMo catalysts for thiophene HDS and found that different Si/Al molar ratios of Al-MCM-41 lead to different nature and concentration of active phases.

[1] The text was submitted by the authors in English.

Table 1. Composition of the catalysts

Catalyst	Al, wt %	W, wt %	Ni, wt %
NiW	0	20	2.5
NiW/Al-1	1	20	2.5
NiW/Al-2	2	20	2.5
NiW/Al-4	4	20	2.5

Venezia et al. [18] reported the effect of Al contents of Al-MCM-41 support on the Pd catalysts for HDS of thiophene and found that the catalyst with Si/Al = 169 showed the highest HDS activity. However, the effect of the Al content in the mesoporous Al-MCM-41 on the HDN activity of Al-MCM-41supported NiW catalyst has not been explored.

In the present paper, a series of Al-MCM-41 supports with different Al contents were prepared by a simple and quick incipient wetness impregnation method, followed by the deposition of Ni and W oxides on these supports by co-impregnation. The catalytic performance of HDN for quinoline on the catalysts was investigated. The systematic study of HDN functionalities of NiW supported on Al-MCM-41 with various Al contents were also explored.

EXPERIMENTAL

Catalyst Preparation

The MCM-41 was provided by the Catalyst Plant of Nankai. The Al-MCM-41 supports with different Al contents (1, 2, or 4 wt %) were prepared through an incipient wetness impregnation method by using appropriate concentration of aluminium isopropoxide (99%, Aldrich) solution in isopropanol on MCM-41. The impregnated samples were dried overnight at 80°C and then calcined at 550°C for 6 h in static air of a furnace. The Al-MCM-41 supports with Al content of 1, 2, 4 wt % were denoted as Al-1, Al-2, Al-4, respectively.

The NiW/Al-MCM-41 catalysts with different Al contents were prepared through co-impregnation method. The nickel nitrate hexahydrate (analytical grade) and ammonium paratungstate (analytical grade) were used as Ni and W sources, respectively. The impregnated samples were dried overnight at room temperature and dried at 80°C for 12 h. Finally, the calcination was performed at 540°C for 3 h to obtain the final catalysts . For comparison, the NiW/MCM-41 catalyst was also prepared following the way described above. All the catalysts have the same amounts of WO_3 (20 wt %) and NiO (2.5 wt %). Table 1 listed the composition of the catalysts .

Characterization Techniques

The structural features of the supports and catalysts were analyzed by X-ray diffraction patterns (XRD) using Bruker D8 Advance diffractometer with CuK_α radiation.

N_2 adsorption-desorption measurement were performed on a Tristar-3000 Micromeritics volumetric apparatus, which reports BET special surface area, average pore diameter, pore volume, and adsorption isotherms automatically.

Surface analyses of the samples were performed by XPS using Kratos XSAM800 fitted with an AlK_α source (1486.6 eV). Binding energies (BE) were referenced to the C1s peak (284.8 eV). Quantitative information of surface composition was obtained from integrated peak areas and corresponding atomic sensitivity factors. Surface molar ratio was obtained from the peak area ratios normalized by the corresponding atomic sensitivity factors.

Raman spectra were recorded on a LabRAM HR800 System equipped with a CCD detector at room temperature. The samples were excited bythe 514 nm Ar^+ laser with a power of 1 MW.

H_2-TPR experiments were carried out in a AutoChem II 2920 equipment (Micromeritics, USA) using 0.01 g catalysts for each run. Typically, the catalysts were pretreated in Ar at 550°C for 2 h and then cooled at 30°C. Subsequently, the Ar flow was switched to 10% H_2–Ar mixed gas. The H_2–TPR was started from 30 to 900°C at a heating rate of 10°C/min and simultaneously monitored by a thermal conductivity detector (TCD).

Catalytic Activity

The experiment for the quinoline HDN was performed in a fixed-bed reactor (i.d. = 6 mm). The catalyst (1 g, size 20–40 mesh) was packed in the constant temperature zone of the reactor and pre-sulfided in situ with a feed of 5 vol % CS_2 in *n*-hexane at 400°C and 3 MPa for 3 h. After sulfidation, the feed was switched to the solution containing quinoline in *n*-heptane (0.5 wt % N). The HDN reaction was conducted on the temperature of 350–390°C, at pressure of 4 MPa, WHSV of 2 h^{-1}, H_2/feed volumetric ratio of 1000. The products of reaction were analyzed using a Agilent-5860 gas chromatograph fitted with a FID detector, using a commercial DB-5 column.

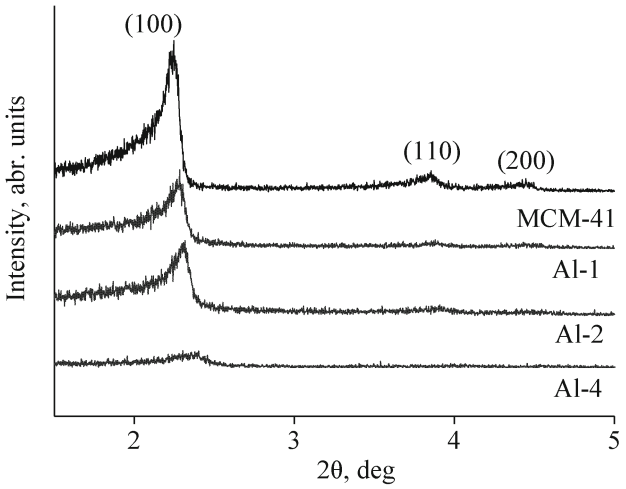

Fig. 1. Small-angle XRD patterns of the supports.

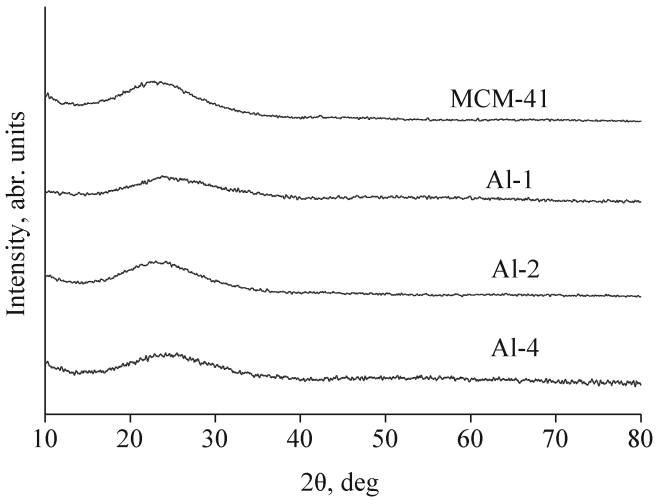

Fig. 2. Wide-angle XRD patterns of supports.

RESULTS AND DISCUSSION

Characterization of Supports

Small-angle XRD. The small-angle XRD patterns of MCM-41 and Al-MCM-41 of different Al contents is shown in Fig. 1. The MCM-41 material displayed a three peak pattern, corresponding to the (100), (110), and (200) diffraction planes, respectively [19]. These peaks are related to a ordered hexagonal pore system. From the Fig. 1, it can be found that the diffraction patterns corresponding to all Al-MCM-41 samples, except Al-4, still exhibited the three peaks assigned to the MCM-41, although with lower peak intensity than bare MCM-41. It showed that the long-range order of the MCM-41 is almost preserved for the Al-MCM-41 samples, except Al-4 [2]. The strong decrease in the peak intensity for the Al-4 sample indicated the loss of long-range order. Therefore, the introduction Al into MCM-41 do not destroy the hexagonal symmetry and only at high Al content the long-range order of the support decreases noticeably.

Wide-angle XRD. Wide-angle XRD technique was used to investigate the presence of any crystallite species in the samples. The wide-angle XRD patterns of the MCM-41 and Al-MCM-41 with different Al contents are shown in Fig. 2. It is demonstrated that the Al species have been highly dispersed on the MCM-41 surface since no diffraction peaks of Al crystalline phases can be found from the XRD patterns of Al-MCM-41 [20]. Furthermore, the XRD patterns show that all the supports exhibit a broad peak caused by the amorphous silica walls.

N_2 adsorption-desorption. The textural properties of the MCM-41 and Al-MCM-41 supports are listed in Table 2. It can be found that the MCM-41 exhibits the highest specific surface area (S_{BET}), pore volume (D_p) and pore diameter (V_p) among all the supports. The Al added to the MCM-41 gives rise to a decrease in S_{BET}, D_p, and V_p, but an increase in the wall thickness (W_p). The decrease in V_p and increase in W_p suggest that some Al species are deposited inside the pore channels of the MCM-41 [21, 22].

The N_2 adsorption–desorption isotherms of the supports are shown in Fig. 3. It shows that all the supports present a type IV isotherm, typical of mesoporous materials. However, as the Al content increases, the height of sharpness loop decreases Al-MCM-41. As the hysteresis loop of isotherms is a result of the actual pore structure, it can be concluded that the structure of Al-MCM-41 is less uniform than that of the purely MCM-41 material. .

Characterization of Catalysts

Wide-angle XRD. The wide-angle XRD patterns of the catalysts are reported in Fig. 4. The absence of peaks

Table 2. Textural properties of the MCM-41 and Al-MCM-41 supports

Sample	S_{BET}, $m^2\ g^{-1}$	D_p, nm	V_p, $cm^3\ g^{-1}$	W_p, nm
MCM-41	1071.00	3.83	1.08	0.97
Al-1	1015.06	3.39	0.90	1.36
Al-2	980.30	3.31	0.91	1.41
Al-4	952.68	2.94	0.77	1.43

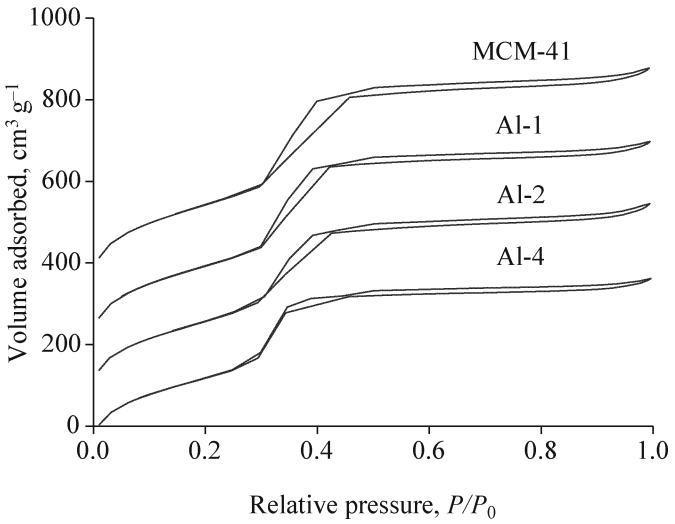

Fig. 3. N_2 adsorption–desorption isotherms of the supports.

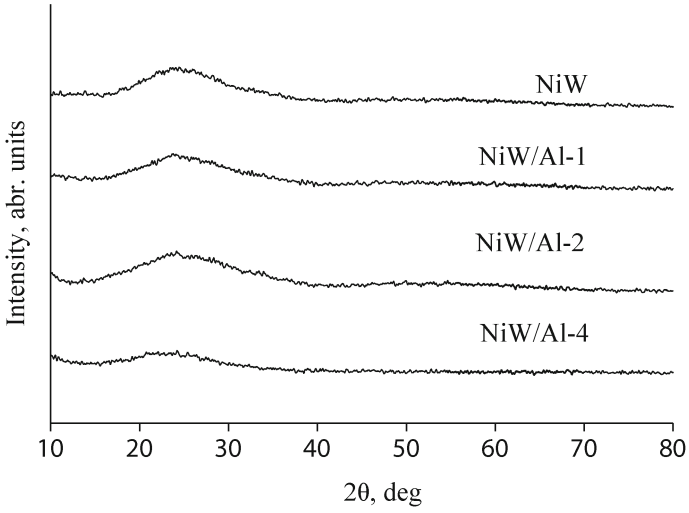

Fig. 4. Wide-angle XRD patterns of catalysts.

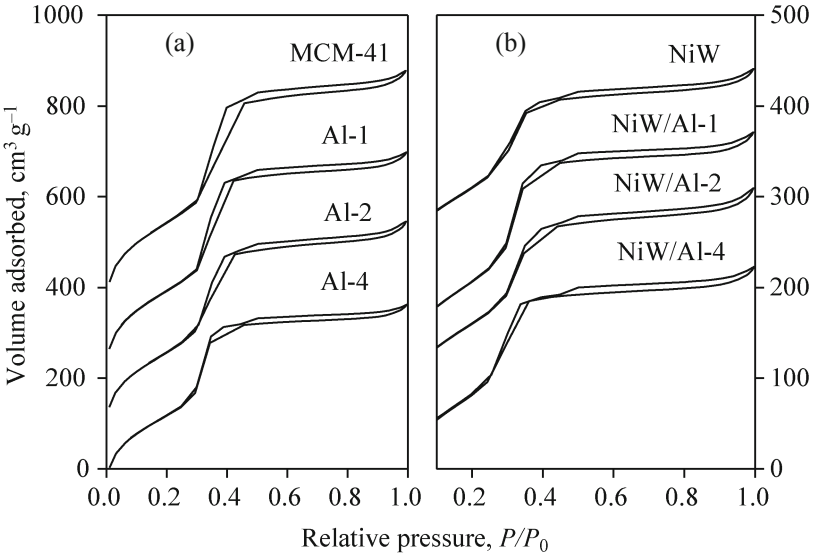

Fig. 5. N2 adsorption-desorption isotherms of (a) supports and (b) catalysts.

due to the Al, Ni, and W crystalline phases in the XRD patterns of all the catalysts reveals that the particle size of Al, Ni, and W crystallites is well dispersed into the support or very small.

N_2 Adsorption-desorption. The textural properties and N_2 adsorption-desorption isotherms of catalysts are given in Fig. 5 and Table 3, For comparison, the textural properties and N_2 adsorption–desorption isotherms of supports are given. From the Fig. 5, it can be found that the step sharpness of the catalysts is much lower than that of the supports, which indicates that the structure is destroyed significantly by impregnation with water solution of Ni and W, especially the catalysts of NiW and NiW/Al-4. From the Table 3, it can be found that the S_{BET} and V_p decrease significantly after the corporation of Ni and W on the supports. This may be due to the blockage and occupation of pores by the Ni and W species.

Raman spectra. Raman spectroscopy is an important tool for obtaining detailed information about the metal oxides phase. In the present work, this technique is used to study the effect of Al on the nature of metal oxide phase of NiW catalysts. The Raman spectra of catalysts are

Table 3. Textural properties of the catalysts and supports

Sample	S_{BET}, $m^2\ g^{-1}$	D_p, nm	V_p, $cm^3\ g^{-1}$	W_p, nm
Al-1	1015.06	3.39	0.90	1.36
Al-2	980.30	3.31	0.91	1.41
Al-4	952.68	2.94	0.77	1.43
NiW	601.09	3.05	0.44	–
NiW/Al-1	575.39	3.35	0.53	–
NiW/Al-2	597.78	3.27	0.49	–
NiW/Al-4	593.54	2.89	0.48	–
MCM-41	1071.00	3.83	1.08	0.97

Table 4. The binding energies of the W4f, Ni2p

Catalyst	Binding energy, eV			
	$W4f_{7/2}$	$W4f_{5/2}$	$Ni2p_{3/2}$	$Ni2p_{1/2}$
NiW	35.7	37.8	856.0 862.3	873.9 880.6
NiW/Al-1	35.8	38.1	855.7 862.1	873.6 880.4
NiW/Al-2	35.9	38.0	855.9 862.3	873.8 880.3
NiW/Al-4	35.8	37.9	855.6 862.0	873.2 879.6

presented in Fig. 6. From the literature data, the MCM-41 does not exhibit band, the bands of 804, 710 and 274 cm^{-1} is ascribed to the crystalline WO_3 presents [23], while the band of 970 cm^{-1} is ascribed to the W=O band in octahedral polytungstate species. Moreover, the band of 883 cm^{-1} is ascribed to the $NiWO_4$, a shoulder at around 811 cm^{-1} reflects the Ni–W–O stretching vibrations [24].

Figure 6 shows that the band assigned to the octahedral polytungstate species (970 cm^{-1}) is observed for all the catalysts and its intensity is higher for the catalysts with Al than that for the catalyst of NiW. Furthermore, the bands assigned to crystalline WO_3 (804 and 710 cm^{-1}) and $NiWO_4$ (883 cm^{-1}) are observed for the catalyst of NiW. On the contrary, no bands assigned to them are observed for the catalysts with Al, whereas a shoulder assigned to the Ni–W–O (811 cm^{-1}) species is observed. Hence, the Al added to the MCM-41 facilitates the formation of octahedral polytungstate species and the Ni–W–O species. This may be as a result of the stronger interaction between W species with the Al_2O_3 than that with silica. The octahedral polytungstate species and Ni–W–O species are precursors of active species for hydrotreating catalyst. Hence, the Al added to the MCM-41 facilitates the formation of the suitable W species on the catalysts.

XPS spectra. The chemical state and surface composition of catalysts were proved by XPS.

The binding energies (BE) of the Ni, W, the ratios of Ni/Si, W/Si, Si/Al are compiled in Table 4. It can be seen that all the catalysts showed similar BE of W4f and Ni2p, suggesting no significant changes of the chemical state for W and Ni species. The doublet peak of $W4f_{7/2}$ and $W4f_{5/2}$ electrons are exhibited at BE position of 35.7–35.9 and 37.8–38.1 eV, respectively. According to the literature, the BE of $W4f_{7/2}$ spectrum around 35.8 and 38.0 eV can be ascribed to WO_3 and/or $NiWO_4$ [25]. The doublet peak of $Ni2p_{3/2}$ and $Ni2p_{1/2}$ electrons are exhibited at BE position of 855.6–856.0 and 873.2–873.9 eV, with the corresponding shake-up satellite at 861.9–862.3 and 879.6–880.6 eV. According to the literature, the BE of $Ni2p_{3/2}$ spectrum in the range of 855.6–856.2 eV ascribes to Ni_2O_3 and/or $NiWO_4$ [26].

The surface molar ratio by XPS analysis can provide the important information about the dispersion of metal species on the catalysts [27]. Table 5 lists the molar ratios of Ni/Si, W/Si, Si/Al on the catalyst. The surface molar ratios of W/Si and Ni/Si of all catalysts are higher than in the bulk. The result indicates that more W and Ni species were distributed on the surface than they were in the bulk

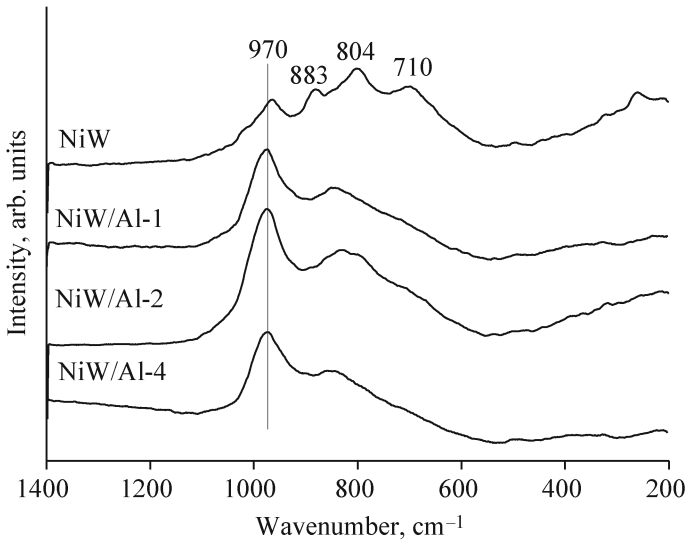

Fig. 6. Raman spectra of catalysts.

Table 5. The ratios of W/Si, Ni/Si and Si/Al on catalysts

Catalyst	Surface composition[a]			Bulk composition[b]		
	W/Si	Ni/Si	Si/Al	W/Si	Ni/Si	Si/Al
NiW	0.073	0.037	–	0.067	0.026	–
NiW/Al-1	0.084	0.067	25.585	0.068	0.026	64.912
NiW/Al-2	0.145	0.062	19.383	0.069	0.027	32.032
NiW/Al-4	0.094	0.064	6.026	0.071	0.027	15.592

[a] Determined by XPS. [b] Calculated number based on the starting material used.

[28]. Moreover, the surface molar ratio of Si/Al on the catalysts is lower than the expected bulk Si/Al molar ratio, suggesting that the catalysts with Al reveals an enrichment of Al on the surface of the catalysts. The surface molar ratios of Ni/Si and W/Si on the catalysts with Al are higher than that on the catalyst of NiW, especially the surface molar ratio of Ni/Si. Thus, it can be concluded that the Al added to MCM-41 can promote the dispersion of W and Ni species on the catalysts. Furthermore, the surface molar ratio of W/Si on the catalysts follows the order of NiW/Al-2 (0.145) > NiW/Al-1 (0.094) > NiW/Al-4 (0.084) > NiW (0.073), indicating that the dispersion of W species increased and then decreased with increasing the content of Al in the range studies. However, the surface molar ratio of Ni/Si on the NiW/Al-MCM-41 catalysts has not changed significantly.

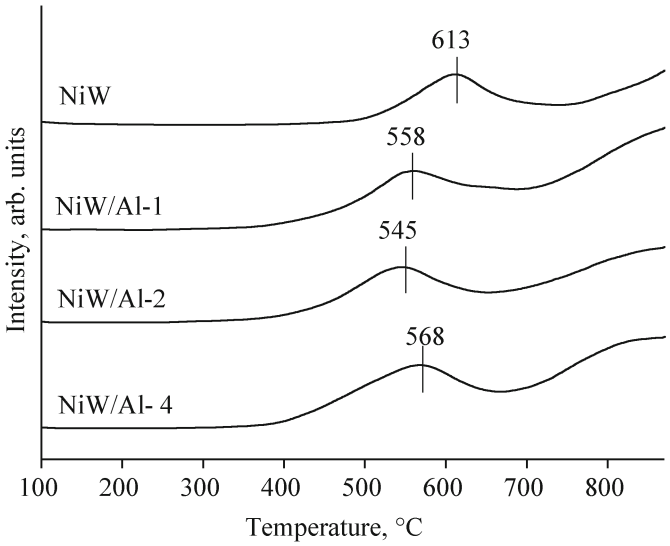

Fig. 7. The H_2-TPR spectra of the catalysts.

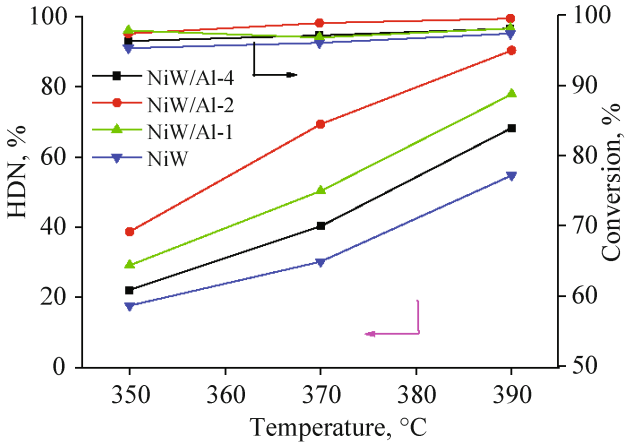

Fig. 8. Conversion and HDN of quinoline for catalysts.

H_2-TPR spectra. The reducibility of the catalysts was characterized by H_2-TPR experiment. Reduction profiles of the catalysts are presented in Fig. 7. All catalysts show two principal reduction peaks in the temperature ranges of 500–700°C and >800°C, respectively. The low temperature peak (500–700°C) can be ascribed to the step of reduction (from W^{6+} to W^{4+}) of octahedral tungsten species with different degrees of polymerization, weakly bound to the support surface. The broad peak at high temperature (>800°C) can be assigned to the second step of the polymeric octahedral W species (from W^{4+} to W^0) and to the first step of reduction of isolated tetrahedral W^{6+} species, which are in strong interaction with the support [29, 30]. Moreover, the maximum reduction temperature of the catalysts in the temperature range of 500–700°C follows the order of NiW (613°C) > NiW/Al-4 (568°C) > NiW/Al-1 (558°C) > NiW/Al-2 (543°C), indicating that the Al added to MCM-41 leads to an easier reduction of polymeric octahedral tungsten species on the catalysts. The decrease in reduction temperature favors for the reduction and sulphidation of the W species leading to the formation of more active species. Moreover, in the TPR profiles of supported NiW catalysts one would expect reduction of NiO species appearing in 150–400°C temperature range, but it is not the case of our catalysts.

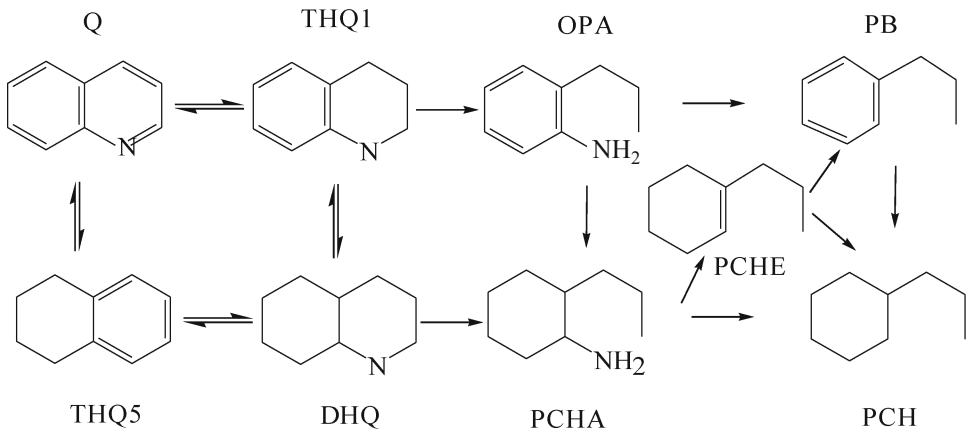

Fig. 9. HDN reaction network of quinoline. (Q) Quinoline, (THQ5) 5,6,7,8-tetrahydroquinoline, (DHQ) decahydroquinoline, (THQ1) 1,2,3,4-tetrahydroquinoline, (OPA) *ortho*-propylaniline, (PCHA) 2-propylcyclohexylamine, (PCHE) propylcyclohexene, (PCH) propylcyclohexane, (PB) propylbenzene.

The phenomenon is probably due to the presence of well-dispersed active components and absence of well-defined bulk species, interacting with the support surface [26].

Activity of catalysts. Figure 8 showed the conversion and HDN of quinoline. It clearly shows that the conversion of quinoline is about 95–99 % for all the catalysts, suggesting that quinoline could be hydrogenated easily. Figure 8 also shows that the HDN activity for all the catalysts increases with increasing reaction temperature. The HDN activity for quinoline follows the order: NiW/Al-2 > NiW/Al-1 > NiW/Al-4 > NiW. The catalyst of NiW/Al-2 presents the highest HDN activity of 38% at 350°C and 90% at 390°C, whereas the catalyst of NiW presents the lowest HDN activity of 17 % at 350°C and 55% at 390°C.

The HDN reaction network of quinoline is presented in Fig. 9. In general, there are two pathways to remove the nitrogen atom from quinoline: hydrogenolysis pathway (pathway I, THQ1 → OPA → PB) and the hydrogenation pathway (pathway II, DHQ → PCHA → PCHE → PCH) (Fig. 9) [31]. Usually, the PCH/PB ratio is supposed to represent the selectivity of the two pathways [32].

The product distribution of HDN for quinoline over the catalysts of NiW/Al-2 and NiW is compared in Fig. 10. For both catalysts, the main intermediates are THQ1, THQ5, DHQ. The main final products are PCH

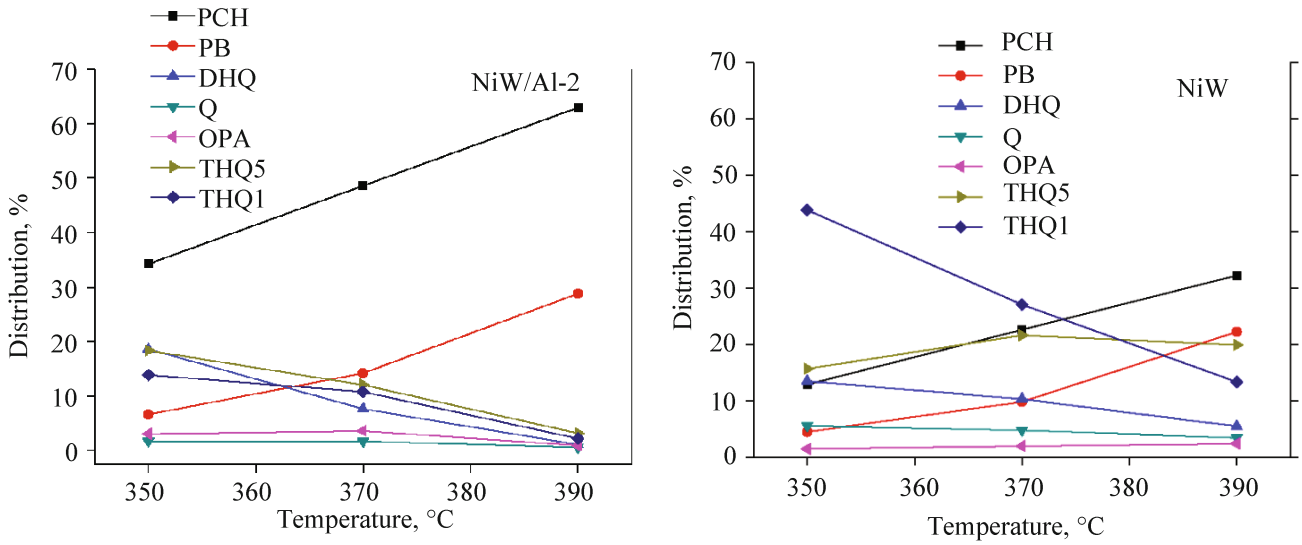

Fig. 10. The distribution of HDN of quinoline for catalysts.

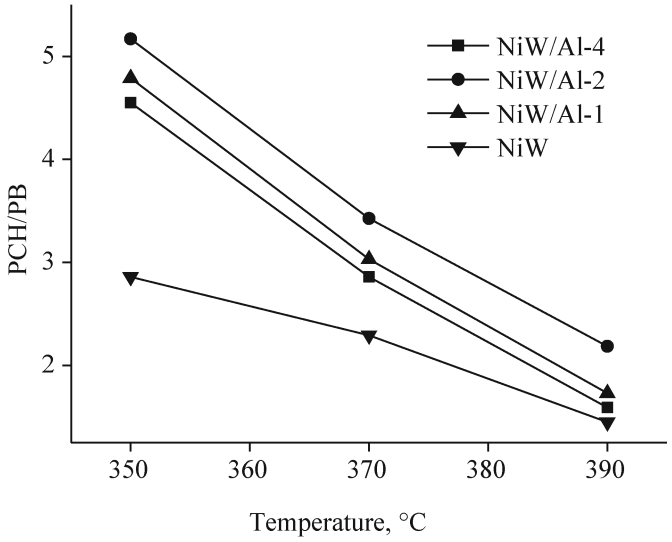

Fig. 11. The ratio of PCH/PB for catalysts.

and PB, especially PCH. For the catalyst of NiW, THQ1 was the primary product of quinoline HDN at 350°C. The selectivities of THQ1 and DHQ decrease straightly with the increase of reaction temperature, accompany with the THQ5 selectivity increasing, reaching maximum, then dropping. The selective of OPA remains constant of about 2%, over the temperature range. The selectivities of PCH and PB increase with the increase in reaction temperature. For the catalyst of NiW/Al-2, the selectivities of THQ1, THQ5, and DHQ decrease with the increase in reaction temperature, accompanying with the increase in the selectivities of PCH and PB.

The PCH/PB ratio of HDN for quinoline over different catalysts is presented in Fig. 11. It follows the order of NiW/Al-2 > NiW/Al-1 > NiW/Al-4 > NiW. It is indicated that, the beneficial effect of the Al added to MCM-41, pathway II is much more preferable than pathway I. Moreover, the tendency of PCH/PB ratio is the same as the tendency of HDN activity over different catalysts. It indicated that the effect of the incorporation Al into MCM-41 of to PCH/PB ratio and HDN activity is consistent. Figure 11 also shows that the PCH/PB ratio for all the catalysts decreases with the increasing the reaction temperature. The result is in accordance with those of M. Jian and R. Prins [30] This because the higher reaction temperature favored the formation of PB [33].

Catalyst activity-structure correlation. The activities of the catalysts have been correlated with the physicchemical properties. The dispersion and W phase on the supports were clearly revealed by the Raman spectra of the catalysts. The presence of WO_3 peak suggests agglomeration of WO_3 species on the support surface leading to the formation of bulk WO_3. According to Raman experiments the NiW catalyst shows the crystalline WO_3 and $NiWO_4$ indicates the poor dispersion of W species due to the inhomogeneous distribution of WO_3. The Al added to the MCM-41 enhances the formation of octahedral polytungstate species and the Ni–W–O species, moreover, the NiW/Al-2 catalyst shows the highest intensity of octahedral polytungstate species and the Ni–W–O species, demonstrating the highest HDN activity. Moreover, the dispersion of W and Ni were also revealed by the XPS. The Al added to the MCM-41 can promote the dispersion of W and Ni on the catalysts.

A better reducibility of the catalysts will be also an indication of an increased number of sulfide species after sulfidation. According to TPR experiments the NiW catalyst shows the highest reduction temperature, demonstrating the lowest HDN activity. The Al added to MCM-41 leads to a decrease in the reduction temperature of polymeric octahedral tungsten species, moreover the NiW/Al-2 catalyst shows the lowest reduction temperature, demonstrating the highest HDN activity.

CONCLUSIONS

In the present work, a series of Al-MCM-41 molecular sieves with different Al contents were prepared by a simple and quick incipient wetness impregnation method. The NiW catalysts supported on these mesoporous supports were prepared by co-impregnation method. It was found that Al content had crucial effect on the physicochemical properties of Al-MCM-41, and then influenced the catalytic performance of catalysts in the HDN of quinoline. The experimental results proved that the NiW/Al-2 catalyst demonstrated the highest HDN activity and PCH/PB ratio among other three catalysts. This may be a consequence of the higher dispersion of W and Ni species, the lower reduction temperature of W species, and the suitable W species on the NiW/Al-2 catalyst.

REFERENCES

1. Klimova, T., Peña, L., Lizama, L., Salcedo, C., and Gutiérrez, O.Y., *Ind. Eng. Chem. Res.*, 2009, no. 48, pp. 1126–1133.
2. Suresh, C., Santhanaraj, D., Gurulakshmi, M., Deepa, G., Selvaraj, M., Sasi Rekha, N.R., and Shanthi, K., *ACS*

Catal., 2012, no. 2, pp. 127−134.

3. Rayo, P., Ramírez, J., Rana, M.S., Ancheyta, J., and Aguilar-Elguézabal, A., *Ind. Eng. Chem. Res.*, 2009, no. 48, pp. 1242–1248.
4. Montesinos-Castellanos, A., and Zepeda, T.A., *Micropor. Mesopor. Mater.*, 2008, no. 113, pp. 146–162.
5. Wang, A.J., Wang, Y., Kabe, T., Chen, Y.Y., Ishihara, A., and Qian, W.H., *J. Catal.*, 2001, no. 199, pp. 19–29.
6. Ling, T.-R., Wan, B.Z., Lin, H.P., and Mou, C.Y., *Ind. Eng. Chem. Res.*, 2009, no. 48, pp. 1797–1803.
7. Li, X., Wang, A.J., Sun, Z.C., Li, C., Ren, J., Zhao, B., Wang, Y., Chen, Y.Y., and Hu, Y.K., *Appl. Catal. A: Gen.*, 2003, no. 254, pp. 319–326.
8. Lu, M.H., Wang, A.J., Li, X., Duan, X.P., Teng, Y., Wang, Y., Song, C.S., and Hu, Y.K., *Energy & Fuels*, 2007, no. 21, pp. 554-560.
9. Méndez, F.J., Llanos, A., Echeverría, M., Jáuregui, R., Villasana, Y., Díaz, Y., Liendo-Polanco, G., Ramos-García, M.A., Zoltan, T., and Brito, J.L., *Fuel*, 2013, no. 110, pp. 249–258.
10. Wang, A.J., Wang, Y., Kabe, T., Chen, Y.Y., Ishihara, A., Qian, W.H., and Yao, P.J., *J. Catal.*, 2002, no. 210, pp. 319–327.
11. Wang, A.J., Ruan, L.F., Teng, Y., Li, X., Lu, M.H., Ren, J., Wang, Y., and Hu, Y.K., *J. Catal.* 2001, 2001, no. 199, pp. 19-29.
12. Silva-Rodrigoa, R., Calderón-Salasa, C., Melo-Bandaa, J.A., Domínguezb, J.M., and Vázquez-Rodríguezb, A., *Catal. Today*, 2004, no. 98, pp. 123–129.
13. Sardhar Basha, S.J., Sasirekha, N.R., Maheswari, R., and Shanthi, K., *Appl. Catal. A: Gen.*, 2006, no. 308, pp. 91–98.
14. Duan, X.P., Li, X., Wang, A.J., Teng, Y., Wang, Y. and Hu, Y.K., *Catal. Today*, 2010, no. 149, pp. 11–18.
15. Franklin, J. M., Oscar, E.F., Xim, B., Dora, A.S., Luis, E., and Tatiana, E.K., *Appl. Catal. B: Environ.*, 2017, no. 219, pp. 479–491.
16. Guo, F., Guo, S.Q., Wei, X.X., Wang, X.X., Xiang, H.W., Qiu, Z.G., and Zhao, L.F., *Catal. Lett.*, 2014, no. 144, pp. 1584–1593.
17. Souza, M.J.B., Marinkovic, B.A., Jardim, P.M., Araujo, A.S., Pedrosa, A.M.G., and Souza, R.R., *Appl. Catal. A: Gen.*, 2007, no. 316, pp. 212–218.
18. Venezia, A.M., Murania, R., La Parola, V., Pawelec, B., and Fierro, J.L.G., *Appl. Catal. A: Gen.*, 2010, no. 383, pp. 211–216.
19. Kraleva, E., Saladino, M.L., Spinella, A., Nasillo, G., and Caponetti, E., *J. Mater. Sci.*, 2011, no. 46, pp. 7114–7120.
20. Wang, Y.D., Shen, B.J.,, Wang, L., Feng, B., Li, J.C., and Guo, Q.X., *Fuel Process. Technol.*, 2013, no. 106, pp. 141–148.
21. Mendoza-Nieto, J.A., Vera-Vallejo, O., Escobar-Alarcón, L., Solís-Casados, D., and Klimova, T., *Fuel*, 2013, no. 110, pp. 268–277.
22. Khdera, A.E.R.S., Hassana, H.M.A., and El-Shall, M.S., *Appl. Catal. A: Gen.*, 2012, no. 411–412, pp. 77-86.
23. Chen, H., Dai, W.L., Deng, J.F., and Fan, K.N., *Catal. Lett.*, 2002, no. 81, pp. 131–136.
24. Zhang, Z.R., Suo, J.S., Zhang, X.M., and Li, S.B., *Appl. Catal. A: Gen.*, 1999, no. 179, pp. 11–19.
25. Cruz-Perez, A.E., Guevara-Lara, A., Morales-Ceron, J.P., Alvarez-Hernandeza, A., Reyes, J.A., Massinc, L., Geantet, C., and Vrinatc, M., *Catal. Today*, 2011, no. 172, pp. 203–208.
26. Palcheva, R., Spojakina, A., Dimitrov, L., and Jiratova, K., *Micropor. Mesopor. Mater.*, 2009, no. 122, pp. 128–134.
27. Cui, G.Q., Wang, J.F., Fan, H.F., Sun, X.Y., Jiang, Y., Wang, S.J., Liu, D., and Gui, J.Z., *Fuel Process. Technol.*, 2011, no. 92, pp. 2320–2327.
28. Ding, L.H., Zheng, Y., Zhang, Z.S., Ring, Z., and Chen, J.W., *Catal. Today*, 2007, no. 125 , pp. 229–238.
29. Wan, G., Duan, A., Zhang, Y., Zhao, Z., Jiang, G., Zhang, D., Liu, J., and Chung, K., *Catal. Today*, 2010, no. 158, pp. 521–529.
30. Lizama, L.Y. and Klimova, T.E., *J. Mater. Sci. Technol.*, 2009, no. 44, pp. 6617–6632.
31. Jian, M. and Prins, R., *J. Catal.*, 1998, no. 179, pp. 18–27.
32. Prins, R., Jian, M., and Flechsenhar, M., *Polyhedron*, 1997, no. 16, pp. 3235–3246.
33. Nguyen, M.T., Tayakout-Fayolle, M., Pirngruber, G.D., Chainet, F., and Geantet, C., *Ind. Eng. Chem. Res.*, 2015, no. 54, pp. 9278–9288.